Analysis of Particle Cloud Height Dynamics in a Stirred Tank

Matthias Eng, Rasmus Jonsson, and Anders Rasmuson
Dept. of Chemical and Biological Engineering, Chalmers University of Technology, SE-412 96, Gothenburg, Sweden

DOI 10.1002/aic.15051
Published online October 1, 2015 in Wiley Online Library (wileyonlinelibrary.com)

Local and temporal variations of the particle cloud formed in a cylindrical mixing vessel were investigated experimentally. Different particle sizes (0.5, 1, and 2 mm) and volumetric concentration up to 20 vol % were evaluated at different impeller speeds. The time-averaged cloud height was linear with impeller frequency and with volume concentration. Suspensions with larger particles had a lower average cloud height, while the standard deviation for the temporal cloud height variation was larger. Two strong periodic phenomena were identified to be dominating the particle cloud height variations. The frequencies were linear with impeller speed, resulting in dimensionless frequencies of S_1=0.02–0.03 and S_2=0.05–0.06. The frequencies were affected by neither the particle size nor the volumetric concentration. The amplitude showed no dependency on the particle size, but the S_2 amplitude significantly decreases and S_1 increases with increasing solid concentration. The results were compared to LES/discrete element method simulations and showed a fair agreement. © 2015 American Institute of Chemical Engineers *AIChE J*, 62: 338–348, 2016
Keywords: cloud height, macroinstabilities, solid-liquid, stirred tank, Computational Fluid Dynamics, Large Eddy Simulation, Euler–Lagrange

Introduction

Solid-liquid suspensions appear in a large amount of chemical engineering applications, for example, crystallization processes and catalytic reactors. Such processes are commonly conducted in agitated mixing vessels. A significant amount of energy is, therefore, needed to lift solid particles off the bottom of the vessel and to keep them suspended in the continuous phase.

Lifted particles often form a cloud, which is clearly separated from the clear liquid layer at the vessel top. The reaction properties in solid-liquid suspensions are dependent on particle distribution and cloud behavior. The well-known Zwietering[1] criterion gives information about the impeller speed and energy needed to achieve "just lift off" conditions for solids concentrations up to 20% by weight, meaning no stagnant particles on the bottom of the vessel.

A particle cloud is often assumed to be of a constant height with certain stationary properties and homogeneous particle distribution. Observations have, however, shown that the particle cloud is not stationary and that the cloud height is characterized by strong temporal and spatial variations.[2] The local particle concentrations and particle residence times inside a stirred vessel may differ by an order of magnitude. For the purposes of process quality and efficiency of solid-liquid suspensions, it is crucial to improve the understanding of flow structures in mixing vessels.

Correspondence concerning this article should be addressed to A. Rasmuson at rasmuson@chalmers.se.

Many studies have investigated the flow structures in single-phase mixing vessels, and the mean flow in different vessel geometries is well understood.[3,4] Instantaneous turbulent flow structures in mixing vessels, however, are very complex and remain a topic of research. Many studies on flow structures in mixing vessels describe the presence of dominant periodic flow instabilities, referred to as Macroinstabilities (MI).[5–10] Macro instabilities are low-frequency phenomena that carry sufficient energy to affect flow structures throughout the vessel. MIs in single-phase systems have been described as linear with impeller speed and, therefore, have a constant Strouhal (S) number. The Strouhal number (S) describes the ratio of frequencies in the flow in comparison to the generating force of the flow. Here the Strouhal number (S) can be seen as the nondimensional frequency between periodic flow frequency (f_{flow}) and impeller revolution frequency (f_{impeller})

$$S=\frac{f_{\text{flow}}}{f_{\text{impeller}}} \tag{1}$$

Studies by Roussinova et al.,[11] using a pitched blade impeller, and Galletti et al.,[12] studying different impeller designs, have identified two dominant MI frequencies at S_{MI}=0.015 and S_{MI}=0.065, while studies by Montes et al.[13] (S_{MI}=0.057) and Eng and Rasmuson[14] (S_{MI}=0.06) using pitched blade impellers, have only identified one dominant MI. Jahoda et al.[15] and Paglianti et al.[16] have described the presence of MIs in the continuous phase of solid-liquid suspensions. Eng and Rasmuson[14,17] have presented detailed findings from research on the frequency and amplitude of MIs in the continuous phase of solid-liquid suspensions agitated by a four-bladed pitched blade impeller, based on experiments[14]

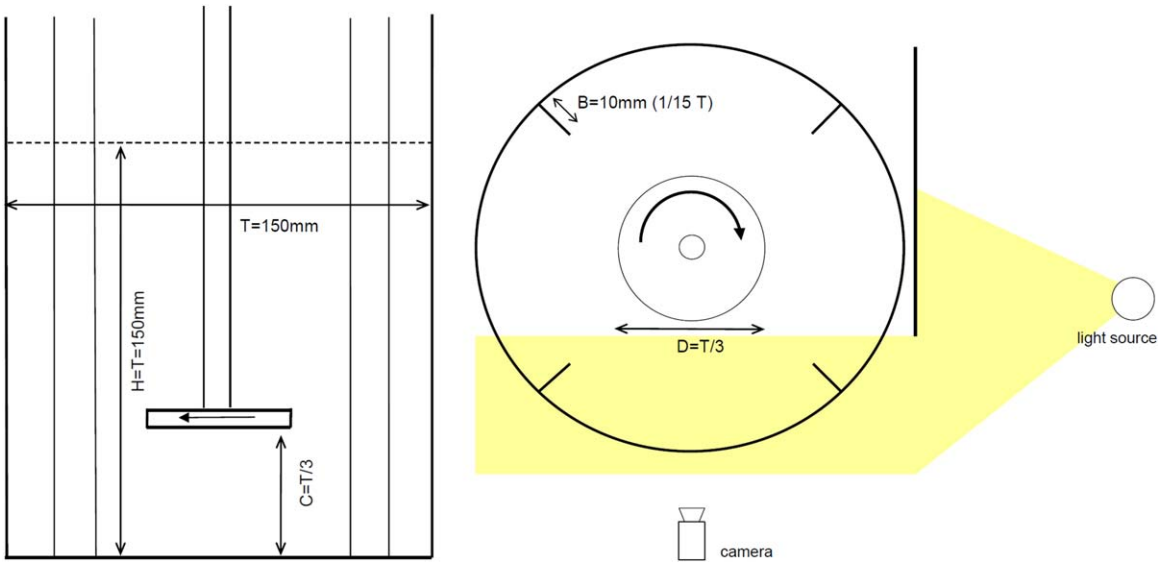

Figure 1. Tank configuration and measurement locations.

[Color figure can be viewed in the online issue, which is available at wileyonlinelibrary.com.]

(concentrations up to 11.8%) and CFD simulations[17] (concentrations up to 3%). The results showed that the MI could be detected in all studied suspensions and that the frequency is not influenced by the addition of solids.

All of these studies have focused on the continuous phase flow and how it is influenced by the presence of particles, only very few studies have been conducted on the dynamic behavior of a particle cloud in a mixing vessel.[18] In a study by Bittorf and Kresta,[18] the development of a particle cloud and the mixing behavior between the particle cloud and the clear liquid layer was investigated. They developed a correlation to predict the cloud height in solid-liquid suspensions agitated by purely axial impellers (HE3 and A310).

The aim of this study is to, in detail, investigate the particle cloud dynamics for different particle sizes and a wide range of concentrations using video techniques and CFD. Periodic phenomena are extracted using spectral analysis.

Flow Configuration

The study was conducted in a model-sized cylindrical mixing vessel with a flat bottom, agitated with a four-bladed pitch-blade impeller (Figure 1). The impeller consists of four flat blades oriented in an angle of 45° to generate a downwards flow.

The vessel had a diameter equal to the filling height of $T=150$ mm, the impeller clearance was fixed to a third of the vessel height at 50 mm ($C=T/3$). The four baffles had a width of 10 mm (1/15 T), the impeller had a diameter of 50 mm ($D=T/3$), which is equivalent to a third of the vessel diameter. The setup was identical to the one used in a previous study of continuous phase spectra.[14] The continuous phase consisted of purified water and the suspended particles were of solid glass with a density of 2500 kg/m^3.

The experimental method is based on high definition videos taken of the mixing vessel to observe particle behavior. To be able to investigate the particle cloud in a specific region, a strong light source was placed at the vessel side and a visor was placed in a way that only the particles closest to the camera position were lit up (Figure 1). Every case was filmed for 30 s with 25 full frames per second at a resolution of 1080 × 1920 (1080p25), resulting in 750 frames. The impeller start-up phase was not investigated, meaning that the impeller was activated and off-bottom suspension was reached before data were recorded.

A total of 68 different configurations were investigated (Table 1). Three different particle diameters were used (0.5 mm/1 mm/2 mm), the impeller speed was varied between 20 Hz (Re=5 × 10^4) and 37.5 Hz (Re=9.4 × 10^4) and the volumetric concentration of solids was varied between 2.5 and 20 vol %. For the 0.5 mm particles a maximum concentration of 15 vol % was possible due to visibility constraints. In this way, all the regions of solid-liquid mixing could be covered from fully dispersed flow to overloaded flow with incomplete off-bottom suspension.

The volumetric concentration describes the average concentration of solids in the vessel (solid-fluid volume ratio). The local particle concentration will vary a lot, and can reach up to the random close packing limit of roughly 60 vol %. Due to the high local particle concentration, interparticle collision was a dominant phenomenon in the particle cloud.

Experimental Methods

The video material was additionally analyzed with a code written in MatLab R2013b. Each video was split into its frames, and the contrast and brightness were adjusted to create a clear separation between the bright particles and the darker

Table 1. Experimental Setup

	2.5 vol %	5 vol %	7.5 vol %	10 vol %	15 vol %	20 vol %
0.5 mm	20	20	25	25	27.5	–
	25	25	27.5	27.5	30	–
	27.5	27.5	30	30	32.5	–
	30	30	32.5	32.5	35	–
1 mm	20	20	25	25	27.5	30
	25	25	27.5	27.5	30	32.5
	27.5	27.5	30	30	32.5	35
	30	30	32,5	32.5	35	37.5
2 mm	20	20	25	25	27.5	30
	25	25	27,5	27.5	30	32.5
	27.5	27.5	30	30	32.5	35
	30	30	32.5	32.5	35	37.5

Values of impeller speed in Hz.

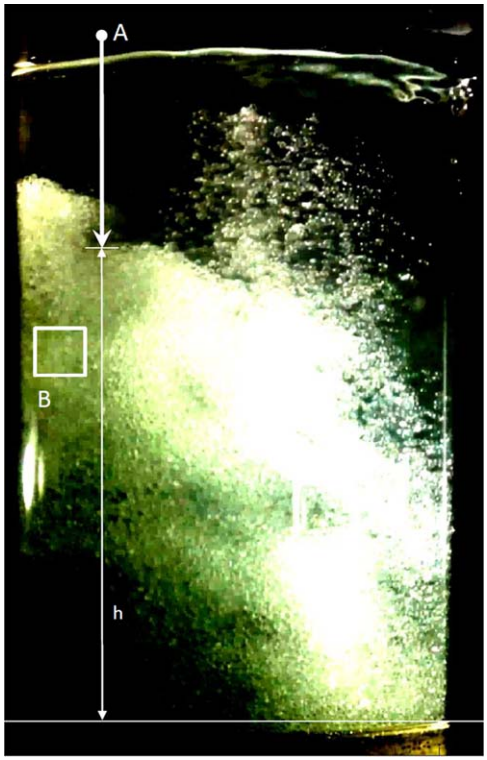

Figure 2. Frame with greater contrast to visualize data collection methods (1 mm 10 vol % 32.5 Hz).

[Color figure can be viewed in the online issue, which is available at wileyonlinelibrary.com.]

continuous phase. Figure 2 shows a sample frame after contrast adjustment. Two methods were developed to investigate cloud dynamics, that is, cloud height and particle density tracking.

Method I: Cloud height tracking

The first method was specifically aimed at cloud height. Cloud height was directly tracked at different locations and at every time step of the video (30 s/25 fps). The algorithm used in the first method counted and evaluated the pixels in one vertical line from the top of the vessel downwards in each frame. "A" symbolizes this method in Figure 2. Nonblack pixels were counted until the brighter particle region was reached. To minimize error and false detection of single particles or dust, the code required 200 nonblack pixels (1.67 cm) in a row as a threshold. The method was applied at 4 different locations, but besides Figure 4, only data from the location closest to the windward side of the baffle (the left-hand side in Figure 2) were used for the final results. This location is comparable to the measurement locations of the continuous phase instabilities by Eng and Rasmuson,[14] where it was found that the continuous phase MI was most pronounced.

Method II: Particle density tracking

A second method was developed to investigate behavior inside the particle cloud. Stationary cells were created in each frame; the average brightness of the pixels in these cells was determined and collected for all time steps. "B" symbolizes this method in Figure 2. Nine different cells were investigated in three vertical rows, two rows on the windward side of the baffle (on the left in Figure 2), and one additional row on the leeward side of the baffle. Each cell had a size of 200 × 200 pixels, which is equivalent to 16.7 × 16.7 mm, 9 cells covered a region of 50 × 50 mm at a vessel height of z=75–125 mm ($^1/_2H-^2/_3H$). The average brightness can be interpreted as local particle concentration. Variation in the average brightness can, then, be used as an indirect way of measuring variations in local particle concentration. However, absolute values of particle concentration cannot be determined using this method.

Frequency analysis

Both methods deliver time-dependent data with a resolution of 25 per second. The cloud height data contain information about the instantaneous absolute particle cloud height, and this information was, then, given a classic statistic evaluation and a spectral evaluation. The statistic evaluation provided the average cloud height and the standard deviation of the cloud height. It should be mentioned that the averaging was only in time, that is, a different average cloud height and standard deviation could be determined for each location. Figure 3 shows both evaluation steps for one sample case.

The spectral analysis was based on the Lomb algorithm.[19] The Lomb algorithm is similar to the more commonly used Fourier transformation, the main difference is that Lomb uses a "per point" approach instead of "per time." Given this, the Lomb algorithm is able to interpret data which are not evenly spaced in time. Even if the data are evenly spaced in the present study, it was convenient to compare the collected data with a previous study on the behavior of the continuous phase using Laser Doppler Velocimetry.[14] A tested sample case gave identical results using Fourier or Lomb analysis. The

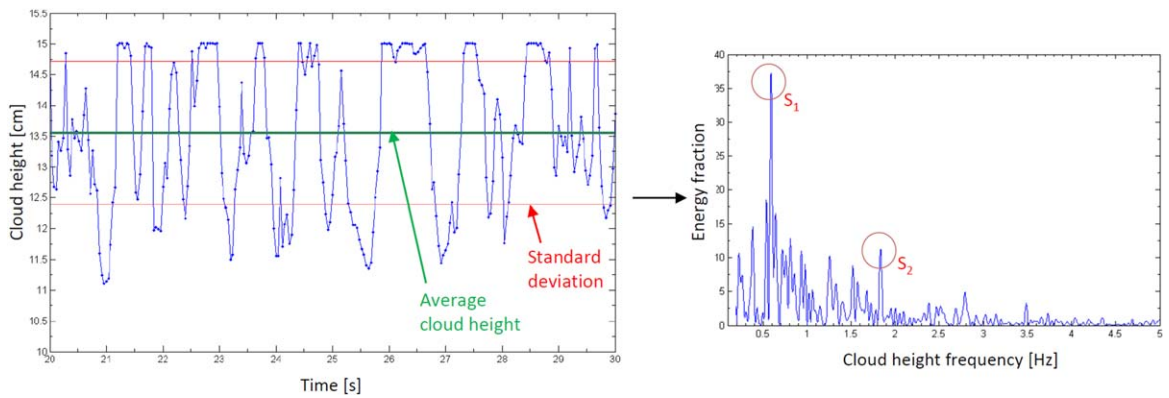

Figure 3. Time-dependent cloud height data and Lomb spectrogram (1 mm 10 vol % 32.5 Hz).

[Color figure can be viewed in the online issue, which is available at wileyonlinelibrary.com.]

Table 2. Setup for Numerical Simulations

Particle diameter	Number of particles	Volume concentration	Mass concentration	Impeller frequency
2 mm	60,000	9.5 vol %	24.3%m	30 Hz
2 mm	37,800	6.0 vol %	15.5%m	30 Hz
1 mm	60,000	1.2 vol %	3.0%m	30 Hz
1 mm	60,000	1.2 vol %	3.0%m	20 Hz

algorithm evaluates the time-dependent data and creates a spectrogram (Figure 3) in which the amplitude represents the energy contained by the corresponding frequency. A strong peak in the spectrogram is equivalent to a large energy fraction of the frequency, which means that the corresponding frequency dominates the flow pattern in the investigated flow. These frequencies can be related to vortex time scales, generally reoccurring flow patterns or periodic instabilities. The Lomb algorithm used is explained in more detail in the previous study by Eng and Rasmuson[14] and by Lomb.[19]

As regard to the significance level, the video tapes of 25 fps make it possible to capture frequencies of 12.5 Hz (half of frame frequency). This would, for a case with impeller speed of 30 Hz, correspond to a dimensionless frequency of 0.41. Peaks started to occur below 0.1 but big peaks appeared mainly at a dimensionless frequency of 0.06 which corresponds to the MI of the current tank setup. The significance level of 95% was calculated to an amplitude of approximately 15.

Numerical Methods

A numerical fluid dynamic model was used to simulate the solid-liquid particle suspension in the mixing tank. The geometry in the CFD simulation was identical to the experimental model tank (Figure 1). The mesh environment of the impeller was modeled with the rotating mesh approach. An LES approach was chosen to model the turbulent flow in the mixing vessel. This comparably complex model is necessary to resolve instationary flow structures sufficiently well to model large-scale instabilities.

CFD model

The CFD model was made up of 25 parts with hexahedral cells and the region closest to the impeller, which had to be modeled with tetrahedral cells. In total, the mesh consisted of 1,151,463 cells with an average subgrid filter length scale of 1 mm. A previously conducted analysis of the Taylor microscale gave values between 1.6 and 0.2 mm, which matches the subgrid filter length scale.[17] Small flow structures must be resolved not only spatially, but also in time, which demands very small time steps. While the time steps, 2×10^{-5} s, are very small, the total simulated time must be comparably large to resolve sufficient periods of macroscaled low-frequency phenomena. To guarantee a reliable frequency analysis it is needed to capture approximately 10 periods of the periodic phenomena. If a MI of 2.2 Hz (continuous phase MI by Eng and Rasmuson[14]) was expected this would lead to an estimated simulated time of at least 4.5 s, which resulted in 225,000 time steps.

The solid phase was modeled using the Lagrangian approach, in which particles are simulated as discrete point sources whose trajectories are computed by solving the force balance. The particles influence the continuous phase through the source terms in the Navier–Stokes formulation, and are affected by the flow through particle drag. To improve the mesh-size dependency of the Discrete Particle Model, a node-based averaging method was used to distribute the source terms over a region of cells. Particle collisions were modeled with a Discrete Element Method, in which all collisions are described with a spring-dashpot model. The numerical simulation was conducted in connection with a previous study,[17] which explains the model in more detail.

Four different cases were simulated and evaluated. Table 2 shows all the cases. Particle size was varied between 1 and 2 mm, and the maximum volumetric concentration investigated was 9.5 vol %. The location data for all particles were exported every 100 time steps, and the location history data were further analyzed with a MatLab code.

Data evaluation

Similar to the experimental data, the particle location data were used to further evaluate the periodic behavior of the particle cloud. Cloud height was tracked by creating a vertical

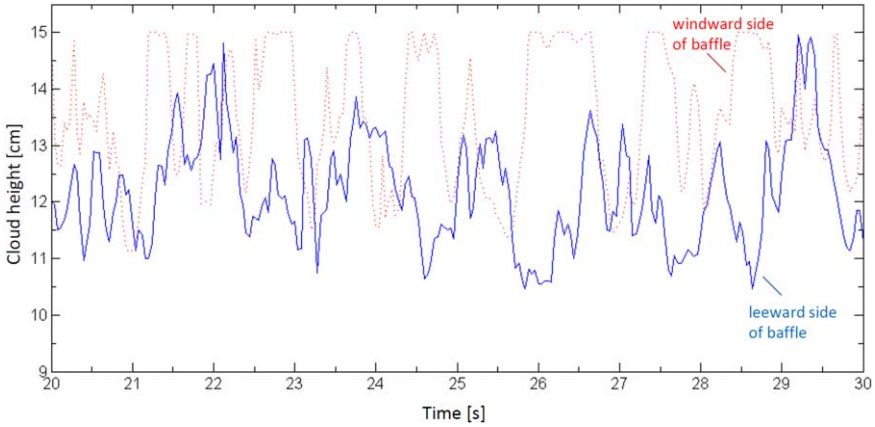

Figure 4. Cloud height variations at different locations in the vessel.

[Color figure can be viewed in the online issue, which is available at wileyonlinelibrary.com.]

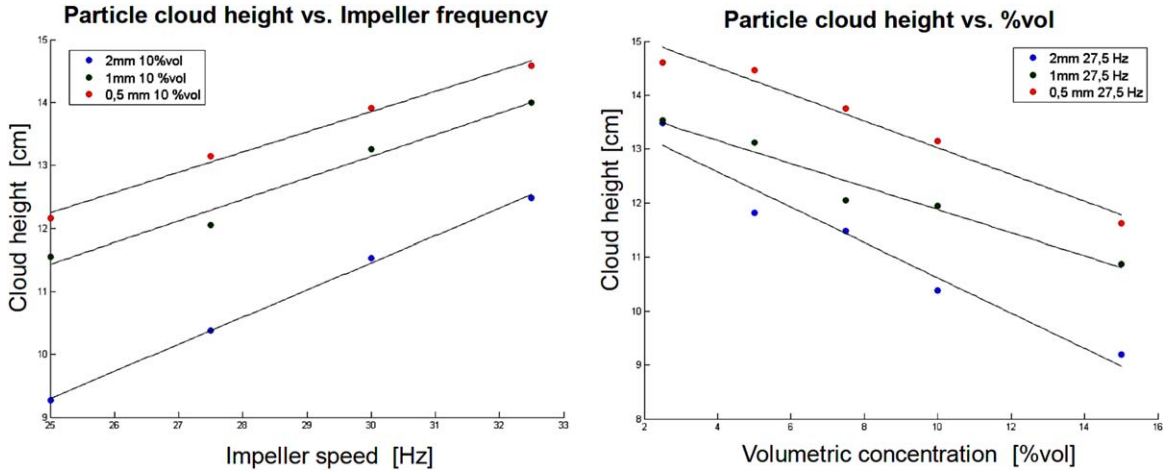

Figure 5. Average cloud height with changing concentration (a) and impeller speed (b).

[Color figure can be viewed in the online issue, which is available at wileyonlinelibrary.com.]

column of cells at the desired position in the vessel. The number of particles contained by each cell was counted by the algorithm, and the cloud height was defined as the vertical location with the steepest gradient or the densest particle concentration. This was repeated for each exported time step, resulting in a resolution of 500 values per second. The position in the vessel was chosen to be approximately the same as in the experimental investigation. Further spectral evaluation of the time-dependent data was conducted using the same Lomb algorithm as in the experimental study. The data from the unsteady Lagrangian simulations contain information of the exact location of all particles at each time step, providing the possibility to track the particle cloud all over the vessel. The vessel was split into 75 × 75 investigation cells, in which the number of particles was counted to determine a local particle concentration. The cloud surface was defined as the z-location at the largest concentration gradient.

Results and Discussion

The particles were generally carried by the continuous phase by means of drag. To keep a large amount of particles

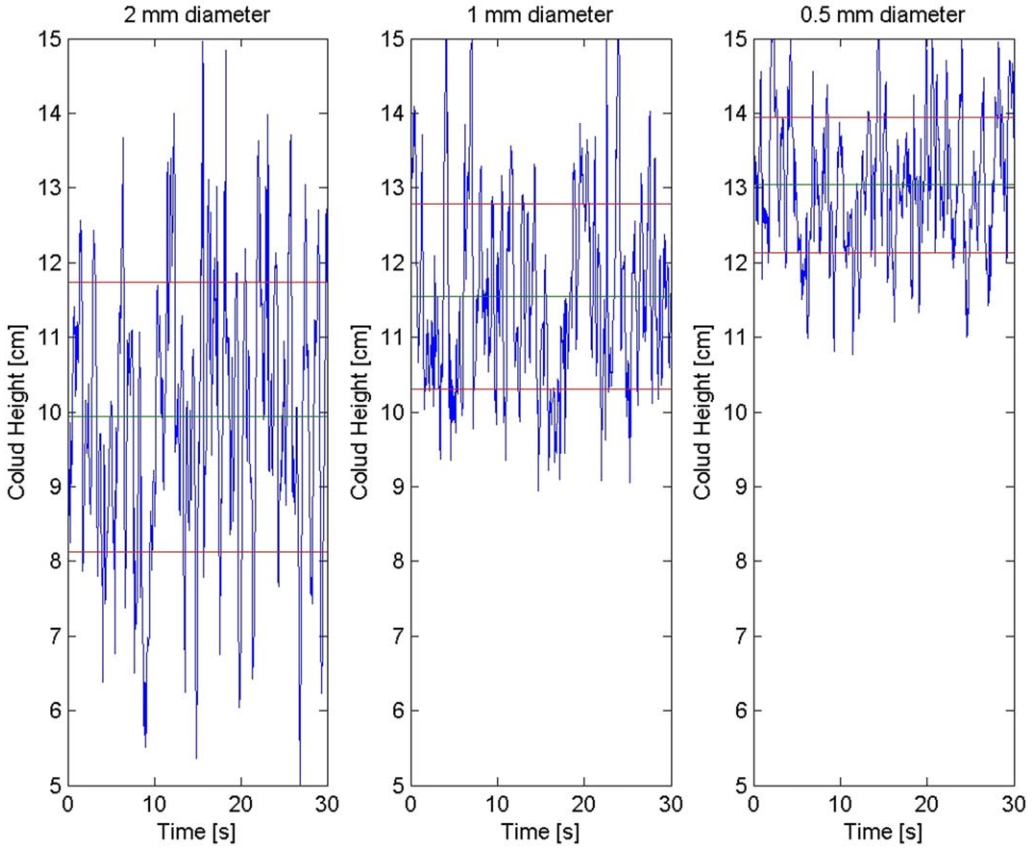

Figure 6. Average cloud height (red) and standard deviation (green) (7.5 vol % at 25 Hz).

[Color figure can be viewed in the online issue, which is available at wileyonlinelibrary.com.]

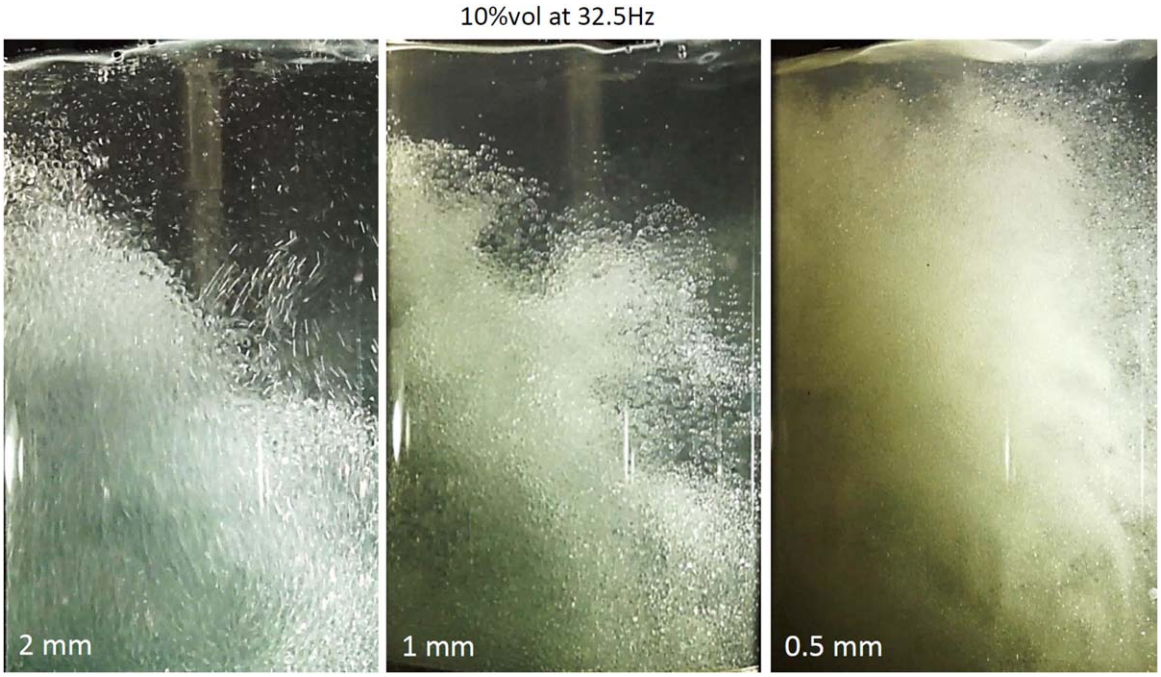

Figure 7. Instantaneous frames of cloud formation with different particles (10 vol % at 32.5 Hz).

[Color figure can be viewed in the online issue, which is available at wileyonlinelibrary.com.]

lifted, the continuous phase exchanged its kinetic energy to the dispersed phase. The flow above the particle cloud was comparably slow and apparently with low turbulence, which may have significant influence on the mixing behavior in the vessel. Similar observations of a clear liquid layer were described by Bittorf and Kresta.[18]

The experimental results confirmed the assumption that the cloud height has great variation in time and space. Figure 4 shows the time-dependent cloud height in a 2.5 vol % 2 mm (20 Hz) suspension tracked at two different locations. It can be seen that the time averages of the cloud height are different for these locations, and that the fluctuation is phase-delayed. This describes the nature of fluctuations in cloud height well; if a particle cloud is at its maximum height in one location it will be close to its minimum height in the opposing location. The baffle jets carry particles higher up, and consequently, the particle cloud is the highest on the windward side of the baffle.

Average cloud height and standard deviation

A clear linear behavior was observed when analyzing the time-averaged particle cloud height at varying impeller speeds. The linear correlation between cloud height and impeller speed was observed at all particle sizes. A clear linear relationship was also observed between the average cloud height and volumetric particle concentration. The cloud height decreased linearly with greater loading. Figure 5 shows the average cloud height at different impeller speeds and particle loadings. Interestingly, Kresta and coworkers[20] observed a similar linear dependency on Reynolds number, when investigating the vertical extent of fully developed turbulence in a single phase mixer.

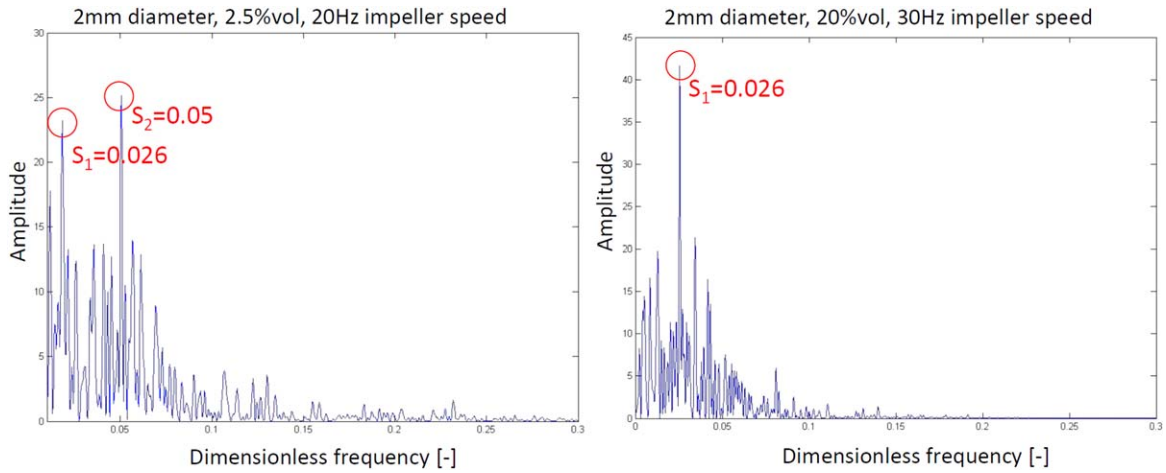

Figure 8. Spectrum of temporal cloud height variation with dominant frequencies.

[Color figure can be viewed in the online issue, which is available at wileyonlinelibrary.com.]

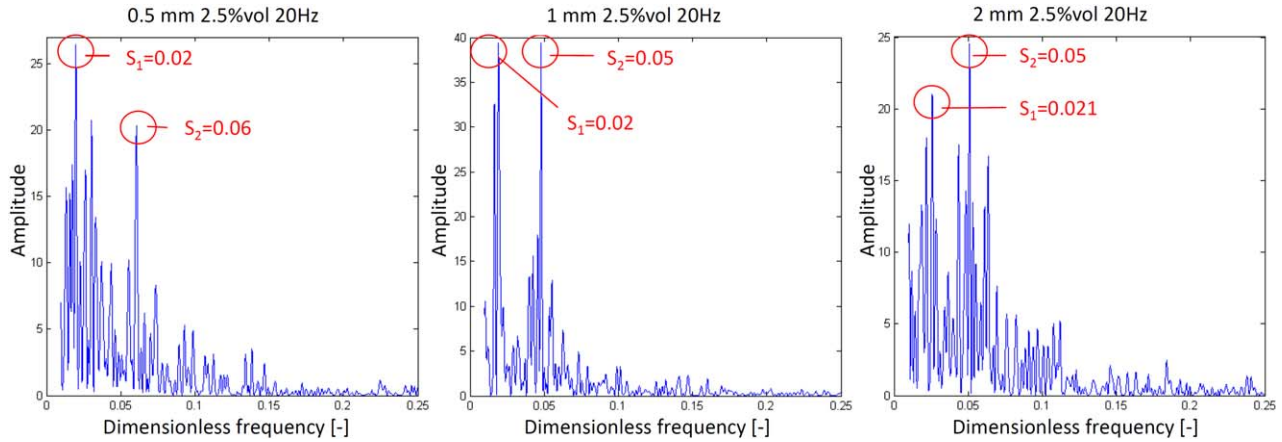

Figure 9. Spectra with dominant frequencies with different particle diameters.

[Color figure can be viewed in the online issue, which is available at wileyonlinelibrary.com.]

Figure 5 also shows the trend that particles with larger diameters cause a lower average cloud height. This trend can be observed throughout all the configurations, however, a linear behavior could not be confirmed. If the standard deviation is added to the analysis, it can be seen that smaller particles cause fewer major fluctuations in particle cloud height (Figure 6). Specifically for the case in Figure 6 with 7.5 vol % at 25 Hz, the standard deviation for the 0.5 mm particles was 0.9 mm, for the 1 mm particles it was 1.25 mm and for the 2 mm particles a standard deviation of 1.85 mm was obtained.

Figure 6 illustrates the connection between particle diameter and average cloud height and the standard deviation of the cloud height. However, while the temporal variation in cloud height decreases with smaller particles, it can be seen in Figure 7 that the particle cloud itself is less clearly pronounced. Large particles have created a clearly defined particle cloud, and only a few particles appear above the defined cloud height. Smaller particles appear more dispersed, the particle cloud is less clearly pronounced and, consequently, it is more likely that the dispersed particles are present above the particle cloud. While larger particles form a stronger local concentration gradient (clear cloud surface), it can be observed that this cloud surface is characterized by larger temporal variations (larger standard deviation).

Figure 7 shows the different particle cloud behaviors with the help of instantaneous particle cloud formations at different particle diameters at identical loading and impeller speed. Smaller particles are more dominated by drag than inertia. This characteristic increases their ability to follow small-scale turbulence vortices and, therefore, they are more likely to be randomly dispersed. Larger particles are more dominated by the mean flow field and macroscaled low-frequency phenomena.

Dominant periodicities of cloud height

The spectral analysis with the Lomb algorithm provided information about the energy content of each frequency in cloud height data. For all configurations (68) the frequency peaks which exceed a certain significance level were plotted and any trend throughout the different configurations investigated. Strong peaks in the spectra indicate significant periodic phenomena in the flow. Most observed cases showed more than one strong peak in the spectrum, and each peak was not always clearly distinguishable. Nevertheless, two reoccurring dominant peaks were outstanding in nearly all cases. It could be observed that the frequencies of these peaks were linearly related to impeller frequency, and therefore, can be described with a constant Strouhal number (S).

The lower of the two dominant frequencies was consistently identified in the frequency regime of S_1=0.02–0.03, the higher frequency occurred between S_2=0.05–0.06. Figure 8 shows two typical spectra including the two dominant frequency

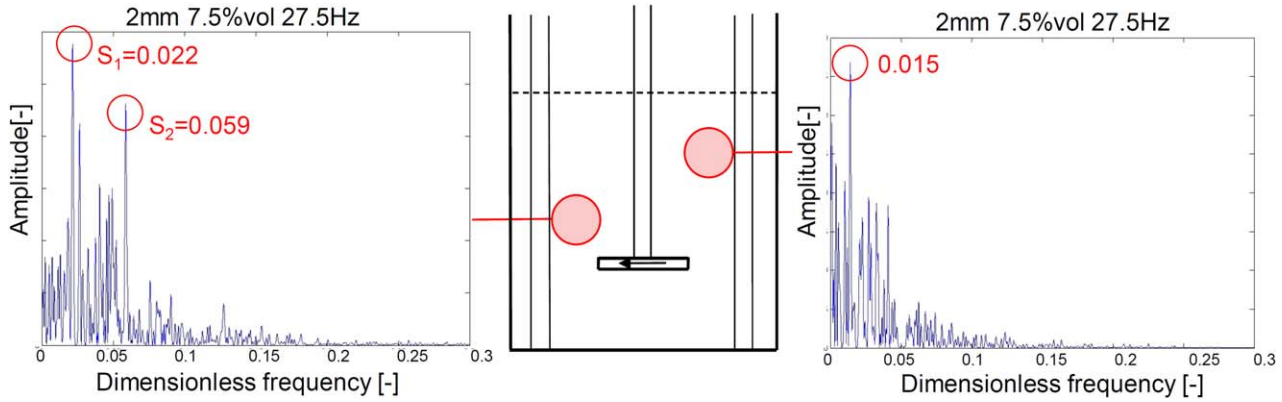

Figure 10. Spectra with dominant frequencies in different vessel regions.

[Color figure can be viewed in the online issue, which is available at wileyonlinelibrary.com.]

peaks. It could be observed by analyzing all spectra, that S_1 and S_2 were the most consistently occurring peaks and described continuous trends with parameter variations.

The frequency of the observed phenomena was not affected by the volume fraction or the size of the particles. Figure 8 presents a comparison of spectra with a ten times larger volume fraction, and it can be seen that the amplitude of the higher frequency S_2 has decreased and is nearly not identifiable anymore while S_1 has increased in amplitude. This can be observed for all particle sizes. The higher impeller speed in Figure 8 was needed to sufficiently suspend the large volume fraction of particles.

Particle size had no effect on the dominant frequencies S_1 and S_2, which means that the same periodic dominance could be identified for all the investigated particle diameters. Figure 9 shows a comparison of spectra at identical impeller speeds and solid loading, but with different particle sizes. Even though Figure 9 shows slight differences between the three sample cases, no particle-size dependency could be identified for either frequency or amplitude.

Strong eruptions at the baffle jets are clearly visible in visual observations, however, they have a very low frequency and they are probably caused by the superposition of other periodic phenomena. They could not be clearly identified in the spectra, which is probably due to their low frequency. Roussinova et al.[11] and Galletti et al.[12] have identified two dominant MI frequencies in a single-phase vessel at $S_{MI}=0.015$ and 0.065. This is similar to the S_1 and S_2 for the particle cloud height in the present study. However, in an identical setup, Eng and Rasmuson[14] have observed only one dominant MI frequency ($S_{MI}=0.06$) of the continuous phase, similar to Montes et al.[13] ($S_{MI}=0.057$). For the particle cloud periodicities in the present study, it is suggested that the lower frequency (S_1) is connected to regular, but weaker eruptions of particles from the cloud into the upper region of the vessel. The higher identified periodicity (S_2) is probably connected to the MI of the continuous phase. Figure 10 illustrates the amplitude of the different Strouhal numbers at different locations in the vessel, which shows additional similarities to the identified MI distribution of the continuous phase.

Bittorf and Kresta[18] and Jahoda et al.[15] have concluded in their studies that the amplitude of the continuous phase is dampened out at higher solid concentrations, and that the MI disappears above the particle cloud. This is in good agreement with the behavior of the particle cloud periodicity S_2, the amplitude of which decreased with increasing volume fraction. This behavior could not be observed for S_1. Nevertheless, the experimental data by Eng and Rasmuson[14] show that the continuous phase MI is present at relatively high solid concentrations and above the cloud height, but with decreased amplitude.

Dominant periodicity of particle density

The second evaluation method (particle density) gives the possibility to analyze periodic behavior at different points inside a particle cloud. Identical energy spectra were obtained when the same location as in the first method (cloud height) was evaluated.

Figure 10 shows a map for the different energy spectra in the particle cloud. It can be seen that dominant large scale periodicities are present at all the investigated locations, and, in nearly all the cases. The second identified periodicity S_2 decreases in amplitude toward the leeward side (right in Figure 10), down to a level at which it cannot be identified as a significant peak. The only remaining dominant peak on the leeward side of the baffle is identified to be around 30% lower than S_1. A similar effect can be observed in the vertical direction as well, in the figure, where the S_2 amplitude is greater in the lower parts of the vessel. Close to the windward side of the baffle (left), at approximately half the vessel height, S_2 has reached its maximum dominance. This coincides with the findings by Eng and Rasmuson[14] and Virdung and Rasmuson,[21] in which a similar distribution of MI amplitude in the continuous phase could be found. Further down in the vessel, it was observed in previous studies[14,21] that the flow of the continuous phase, as well as of suspended particles, is governed by high velocity impeller discharge.

Table 3. Average Cloud Height and Standard Deviation from CFD Simulations

Setup	Average cloud height	Standard deviation
2 mm 9.5 vol % 30 Hz	79 mm	16 mm
2 mm 6.0 vol % 30 Hz	102 mm	26 mm
1 mm 1.6 vol % 30 Hz	93 mm	22 mm
1 mm 1.6 vol % 20 Hz	81 mm	19 mm

Numerical results

The temporal evaluation of cloud height data provides information about time-averaged cloud height and the standard deviation for the different setups, similar to Figure 6. The values from the CFD simulations (Table 3) follow the trend discovered in the experiments well. The case with 9.5 vol % of 2 mm particle was overloaded and full suspension was not achieved.

With the Lagrangian particle location data, it is possible to analyze the local particle concentration in detail. Instead of cloud surface, Figure 11 shows the local particle volume fraction in different horizontal and vertical planes in the vessel. Figure 11 shows the instantaneous information of the 2 mm 9.5 vol % configuration. As can be seen, particle distribution is clearly uneven, and a symmetric pattern at the baffles can be identified. The particle-carrying baffle jets are the main source for particles in the upper region of the vessel. The periodic variation in these baffle jets is the main reason for the dynamics of the cloud height. The large concentration of heavy 2 mm particles was not fully suspended, which is shown by the typical shape of a region with a high volume fraction (>0.3) at the bottom center and at the edges of the vessel.

Due to the large number of solid particles and the very computationally demanding collision model, the simulations took a long time and only 5 s could be simulated. The collection of data started after a steady-state suspension was reached; the same CFD procedure as in Eng and Rasmuson[17] was used. A total time of 5 s (150 impeller revolutions) is equivalent to approximately 9 periods of the S_2 phenomenon at an impeller speed of 30 Hz, which results in 250,000 time steps of which every 100th was sampled. The total simulated time was sufficient to identify the frequencies of dominant periodicities, while a longer simulated time would be preferable to determine the exact energy fraction. For the most demanding case with 60,000 2 mm particles, sufficient time steps could not be simulated to obtain reliable spectral data. The temporal resolved particle location data were evaluated using spectral

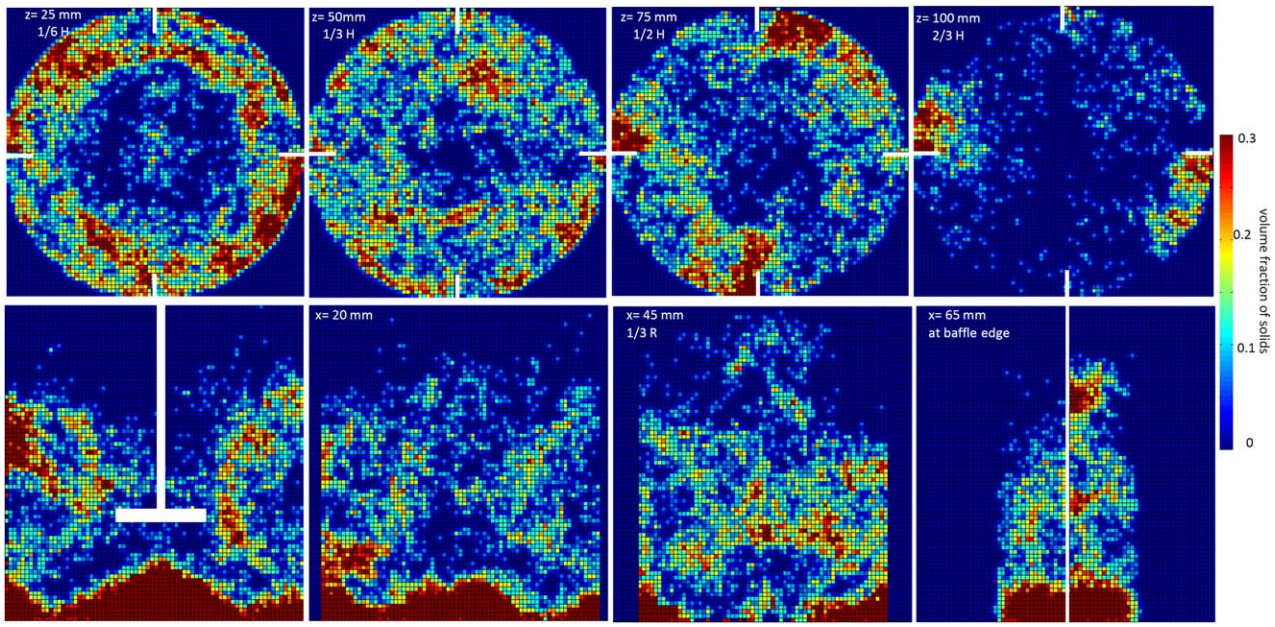

Figure 11. Snapshots of horizontal and vertical planes of particle concentrations (2 mm 9.5 vol %).

[Color figure can be viewed in the online issue, which is available at wileyonlinelibrary.com.]

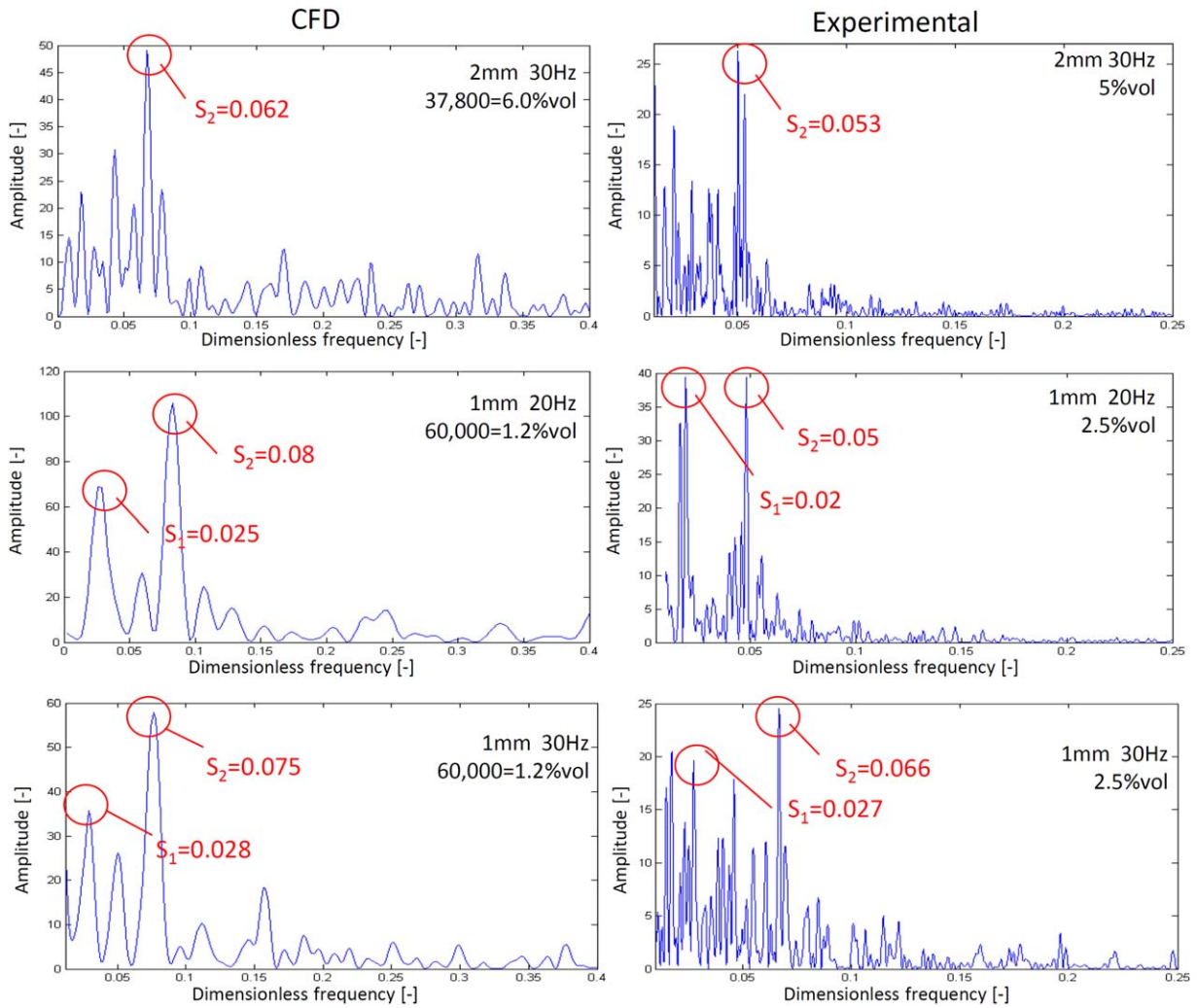

Figure 12. Comparison between CFD simulations and experimental data.

[Color figure can be viewed in the online issue, which is available at wileyonlinelibrary.com.]

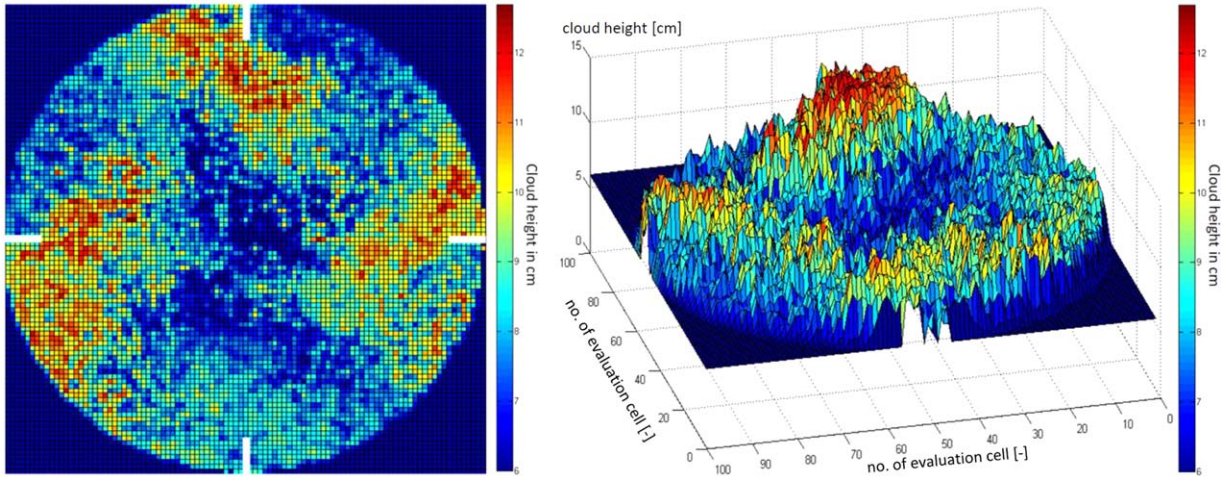

Figure 13. Instantaneous cloud height analysis of CFD data in two different views (2 mm 9.5 vol %).

[Color figure can be viewed in the online issue, which is available at wileyonlinelibrary.com.]

analysis to create Lomb spectra with the dominant periodic behaviors of the particle cloud surface.

Figure 12 presents a comparison of the energy spectra of the cloud height dynamics from the experiments to the spectra obtained using CFD simulations. The CFD spectra all show a certain similarity to the experimental data; a dominant frequency in a range comparable to S_2 could be identified in all the cases. Some cases also showed a lower dominant frequency, similar to S_1. The CFD data created up to 20% higher dominant frequencies than the experiments. Similar results were observed by Eng and Rasmuson[17] in which the MI created using CFD simulations was 10% higher than in the experiments.

The peaks for the higher dominant frequency S_2, are well pronounced in Figure 12, which means that the particle cloud height shows a strong periodic variation in the simulations. The range of dominant frequencies in the simulations and in the experiments is in reasonable agreement. The second dominant frequency could be identified in some cases of numerical simulation, but the total simulated time was too short to draw reliable conclusions from the spectra, in particular regarding the amplitudes and also for much lower frequencies. It should be emphasized the calculations are very time consuming.

The exact particle cloud surface could be tracked with the CFD data. In contrast to the particle concentration plots, it is the height of the cloud surface, rather than the volume fraction, which is identified in this analysis. The cloud height is defined as the location with the largest gradient in volume fraction. Figure 13 shows two instantaneous particle cloud surface plots. It can be seen that the particle cloud is characterized by large differences in height. On the windward side of the baffles, the particle cloud nearly extends up to the vessel surface (150 mm). In the center of the vessel and on the leeward side, the particle cloud does not reach over 1/3 of the vessel height (50 mm).

The surface plots are in good agreement with the volume fraction plots (Figure 11), in which the importance of the baffle jets and the high concentration at the vessel walls are identified. Particles are carried upwards by the baffle jets, these particle-laden jets rotate in a helical shape toward the center of the vessel. This particle cloud shape is in good agreement with observations in the experiments (Figures 4 and 7). Periodic fluctuations in the continuous phase, such as macro instabilities and the related periodic changes in the baffle jets, influence the behavior of the periodic particle cloud.

Conclusions

The study deals with the dynamics of the particle distribution which should be of general importance for a number of applications involving solid suspensions. In particular the dynamics of the particle cloud height is studied and couplings to macro instabilities are observed. The latter are low frequency phenomena that have an impact on the mass-transfer characteristics of the vessel.

With the developed experimental technique it was possible to identify the temporal variations in the height of a particle cloud in a solid-liquid suspension. Different concentrations, impeller speeds and particle sizes were investigated.

The time-averaged cloud height was linear with impeller frequency (Reynolds number) and with volume concentration (Figure 5). Suspensions with larger particles had a lower average cloud height, while the standard deviation for the temporal cloud height variation was larger. At the same time larger particles behave like a dense cloud, while smaller particles are more dispersed and more often occur outside a cloud (Figures 6 and 7).

The analysis of the cloud dynamics revealed a dominating periodic behavior. The identified dominant frequencies were found to be linear with impeller speed, which results in a constant Strouhal number (a dimensionless frequency). The two dominant periodicities could be identified as S_1=0.02–0.03 and S_2=0.05–0.06. They were identified in the spectra of all investigated conditions (Figures 3 and 9). The spectra did not show any particle size dependency, frequency (Strouhal number) and amplitude of the periodicities were unchanged. However, the spectra showed a significant dependency on the particle concentration. While the frequency of the dominant periodicity was unaffected, a strong effect on the amplitudes was observed. An opposing effect for the two periodicities was observed, with increasing particle concentration, the energy fraction of S_1 increased and S_2 decreased (Figure 8). The two periodicities can be related to different phenomena in the particle cloud. The low frequency (S_1) is related to eruptions on the cloud surface that carry particles to the vessel top. S_2 can be related to the continuous phase MI. They can be identified with the same Strouhal number and the decreasing

amplitude at high concentrations is in good agreement with studies regarding continuous phase MI:s.

With the numerical simulations it was possible to evaluate the local particle concentration at any place in the vessel, and to find strong inhomogeneities and temporal variations (Figure 11). The cloud surface could be identified and tracked. The spectral evaluation is very time demanding, especially when the lower frequency region is considered. Nevertheless, the obtained findings show reasonable agreement with the experimental data (Figure 12). Two dominant frequencies were detected, the lower one agreed very well with the S_1 region in the experiments. The second dominant periodicity was detected at slightly higher frequencies than the experimental S_2 region.

Acknowledgments

The computations were performed on resources provided by the Swedish National Infrastructure for Computing (SNIC) at C3SE. Financial support from the Swedish Research Council is gratefully acknowledged.

References

1. Zwietering T. Suspending of solid particles in liquid by agitators. *Chem Eng Sci*. 1958;9:244–253.
2. Sardeshpande M, Juvekar V, Ranade V. Hysteresis in cloud heights during solid suspension in stirred tank reactor: experiments and CFD simulations. *AIChE J*. 2010;56:2795–2804.
3. Paul EL, Atiemo-Obeng VA, Kresta SM. *Handbook of Industrial Mixing*. Hoboken, NJ: Wiley, 2003.
4. Hasal P, Montes J, Boisson H, Fort I. Macro-instabilities of velocity field in stirred vessel: detection and analysis. *Chem Eng Sci*. 2000; 55:391–401.
5. Kresta SM, Wood PE. The mean flow field produced by a 45° pitched blade turbine: Changes in the circulation pattern due to off bottom clearance. *Can J Chem Eng*. 1993;71:42–53.
6. Bruha OI, Forť I, Smolka P. Flow transition in an axially agitated system. In: *Proceedings of VIII European Conference Mixing (Cambridge) IChEME Symposium Series No. 136*, 1994:121–128.
7. Roussinova V, Kresta SM, Weetman R. Low frequency macroinstabilities in a stirred tank: scale-up and prediction based on large eddy simulations. *Chem Eng Sci*. 2003;58:2297–2311.
8. Nikiforaki L, Montante G, Lee K, Yianneskis M. On the origin, frequency and magnitude of macro-instabilities of the flows in stirred vessels. *Chem Eng Sci*. 2003;58:2937–2949.
9. Kilander J, Svensson FJE, Rasmuson A. Flow instabilities, energy levels, and structure in stirred tanks. *AIChE J*. 2006;52:4039–4051.
10. Doulgerakis Z, Yianneskis M, Ducci A. On the interaction of trailing and macro-instability vortices in a stirred vessel-enhanced energy levels and improved mixing potential. *Chem Eng Res Des*. 2009;87: 412–420.
11. Roussinova VT, Kresta SM, Weetman R. Resonant geometries for circulation pattern macroinstabilities in a stirred tank. *AIChE J*. 2004;50:2986–3005.
12. Galletti C, Paglianti A, Lee KC, Yianneskis M. Reynolds number and impeller diameter effects on instabilities in stirred vessels. *AIChE J*. 2004;50:2050–2063.
13. Montes J, Boisson H, Fort I. Velocity field macro-instabilities in an axially agitated mixing vessel. *Chem Eng J*. 1997;67:139–145.
14. Eng M, Rasmuson A. Influence of solids on macro-instabilities in a stirred tank. *Chem Eng Res Des*. 2012;90:1052–1062.
15. Jahoda M, Machon V, Vlach L, Fort I. Macro-instabilities of a suspension in an axially agitated mixing tank. *Acta Polytech*. 2002;42: 3–7.
16. Paglianti A, Montante G, Magelli F. Novel experiments and a mechanistic model for macroinstabilities in stirred tanks. *AIChE J*. 2006; 52:426–437.
17. Eng M, Rasmuson A. Large eddy simulation of the influence of solids on macro instability frequency in a stirred tank. *Chem Eng J*. 2015;259:900–910.
18. Bittorf K, Kresta S. Prediction of cloud height for solid suspensions in stirred tanks. *Chem Eng Res Des*. 2003;81:568–577.
19. Lomb NR. Least-square frequency analysis of unequally spaced data. *Astrophys Space Sci*. 1976;39:447–462.
20. Machado MB, Bittorf KJ, Roussinova VT, Kresta SM. Transition from turbulent to transitional flow in the top half of a stirred tank. *Chem Eng Sci*. 2013;98:218–230.
21. Virdung T, Rasmuson A. Solid-liquid flow at dilute concentrations in an axially stirred vessel investigated using particle image velocimetry. *Chem Eng Commun*. 2007;195:18–34.

Manuscript received Jan. 28, 2015, and revision received Aug. 12, 2015.